European Congress on Computational Methods
in Applied Sciences and Engineering (ECCOMAS 2012)
J. Eberhardsteiner et.al. (eds.)
Vienna, Austria, September 10-14, 2012

APPROXIMATION OF NON-CONVEX ANISOTROPIC ENERGIES VIA WILLMORE ENERGY

Paola Pozzi, Philipp Reiter

Universität Duisburg-Essen
Fachbereich Mathematik, Campus Duisburg, Forsthausweg 2, 47057 Duisburg, Germany
e-mail: {paola.pozzi,philipp.reiter}@uni-due.de

Keywords: non-convex energies, regularization, FEM-discretization, simulations, wrinkles phenomenon

Abstract. *It is well known that material scientists consider evolution equations associated to energy functionals that are not convex. The problem with this approach is that the associated evolution equation becomes forward-backward parabolic. A higher order term is usually added in order to be able to deal with the inherent instability.*

Here we consider a problem within this framework, namely we investigate the gradient flow for an anisotropic area functional characterized by a non-convex weighting function, and regularize it via a Willmore term.

We study the case of one-dimensional graphs. The evolution problem is tackled numerically by considering a suitable finite element scheme and by performing several simulations. The latter allow us to get a feeling about the behavior of the evolution equation when the regularization parameter is sent to zero.

Presenting new simulations and revisiting some experiments from a previous investigation of the authors, we shift our focus on the longtime behavior of the flow.

1 INTRODUCTION

The investigation of planar sharp phase-interface models arising in several applications focuses on the study of evolution equations of type

$$b(\theta)V = (f(\theta) + f''(\theta))\kappa - F, \tag{1}$$

where V is the normal velocity, κ the curvature, θ stands for the angle of the interface normal to some fixed axis, b is a positive map that characterizes the kinetics and measures the drag opposing interfacial motion, f is the interfacial energy, and F is the difference in bulk energy between phases (see [1] and Gurtin's monograph [6]). It is well known that material scientists use energies for which $(f + f'')$ is negative on some intervals (see for instance references given in [7]). The difficulty with this approach is that the associated evolution equation becomes forward-backward parabolic. This problem can be overcome by adding a higher order term, for instance by considering

$$b(\theta)V = (f(\theta) + f''(\theta))\kappa - F - \varepsilon^2(\kappa_{ss} + \tfrac{1}{2}\kappa^3) \tag{2}$$

with $\varepsilon > 0$ small (s is here the arc-length), and by studying the associated fourth order evolution equation (see [1] and [4]).

Here we consider motion of one-dimensional graphs under anisotropic non-convex mean curvature flow regularized via a Willmore term: more precisely we consider the L^2-gradient flow of the energy

$$E_\varepsilon : u \mapsto \int_{\operatorname{graph} u} \gamma(\nu) dA + \varepsilon^2 \int_{\operatorname{graph} u} \kappa^2 dA, \qquad \varepsilon > 0, \tag{3}$$

where κ denotes the curvature of the graph of u, the vector ν its unit normal, and γ is a non-convex anisotropy map. Note that with $\nu = (\cos\theta, \sin\theta)$ and $\gamma(\nu) = f(\theta)$ one easily recovers the evolution equation (2) (with $F \equiv 0$ and $b \equiv 1$) and that the non-convexity of γ is related to the negative sign of $(f + f'')$.

The fourth order evolution equation associated with the flow of the above energy functional (3) takes the form

$$\frac{u_t}{\sqrt{1+u_x^2}} = g''(u_x)u_{xx} - \frac{\varepsilon^2}{(1+u_x^2)^{1/2}}\left(2\frac{u_{xxxx}}{(1+u_x^2)^2} - 20\frac{u_x u_{xx} u_{xxx}}{(1+u_x^2)^3} + \frac{u_{xx}^3}{(1+u_x^2)^4}(30u_x^2 - 5)\right) \tag{4}$$

plus boundary conditions; here g denotes the map $g(y) := \gamma(y, -1)$.

Our ambitious long term plan is to understand this evolution equation in the limit $\varepsilon \to 0$. This is far from being a trivial task (cf. for instance [3], [2] and references therein).

As a first step in this direction we investigated the stationary case [8]. By using simple but beautiful geometric arguments we proved that under suitable assumptions on the non-convex anisotropy map γ there exist minimizers of E_ε in the class $\mathcal{C}_{\alpha,\beta} \cap H^{2,2}(0,1)$ where

$$\mathcal{C}_{\alpha,\beta} := \{u \in H^{1,1}(0,1) \,:\, u(0) = \alpha, u(1) = \beta\}, \qquad \alpha, \beta \in \mathbb{R}. \tag{5}$$

Moreover we were able to state that, for sufficiently small ε, minimizers are either concave or convex and that a sequence of convex minimizers u_ε for E_ε converges (for $\varepsilon \to 0$) in $H^{1,p}$ $(1 \le p < \infty)$ to a piecewise linear map u, which we can describe accurately (we refer to [8] for more details).

Next we looked at the evolution equation: here we tackled the problem from a numerical point of view, in order to get an idea for what phenomena should be expected in the limit, when the regularization parameter is sent to zero. By means of a finite element discretization we provided a suitable semi-implicit scheme for a mixed formulation (this allows us to use piecewise linear finite elements) and considered several numerical experiments.

In [8] we focussed on the phenomena that appear in the first part of the evolution, where one observes a fast formation of ε-dependent microstructures ("wrinkles").

Here we present first experiments that deal with the evolution after the first big energy drop. To this end we perform an appropriate time rescaling of the flow. We present new simulations and revisit some of our previous tests shown in [8, § 9.3].

Acknowledgements. We would like to thank G. Bellettini, G. Dziuk, and C. M. Elliott for many helpful conversations. This work was partially supported by DFG Transregional Collaborative Research Centre SFB TR 71.

2 PRELIMINARIES AND NOTATION

In the following we consider *non-convex* anisotropy functions $\gamma : \mathbb{R}^2 \to [0, \infty)$, $\gamma \in C^2(\mathbb{R}^2 \setminus \{0\})$, that are positive ($\gamma(p) > 0$ for $p \neq 0$) and positively homogeneous of degree one, that is $\gamma(\lambda p) = |\lambda|\gamma(p)$ for $\lambda \in \mathbb{R}$, $p \in \mathbb{R}^2$. The associated Frank diagram is given by

$$\mathcal{F}_\gamma := \{p \in \mathbb{R}^2 : \gamma(p) \leq 1\}. \tag{6}$$

As mentioned in the Introduction we study the evolution of one dimensional graphs of

$$u : \bar{I} \to \mathbb{R}, \qquad I = (0, 1),$$

for the L^2-gradient flow related to the energy given in (3). Therefore it is natural to define

$$g : y \mapsto \gamma(y, -1) \quad (\in C^2(\mathbb{R}, (0, \infty)), \tag{7}$$

and to express the energy functional as

$$E_\varepsilon : u \mapsto \int_0^1 g(u_x(x)) + \varepsilon^2 \frac{u_{xx}(x)^2}{(1 + u_x(x)^2)^{5/2}}\, dx. \tag{8}$$

For the derivation of a mixed formulation of the flow it is useful to introduce a new map

$$w := \kappa\sqrt{1 + u_x^2} = \frac{u_{xx}}{1 + u_x^2} \tag{9}$$

where $\kappa = u_{xx}(1 + u_x^2)^{-3/2}$ is the curvature of the graph.

Our discretization scheme is based on following *mixed formulation* of the flow: look for $u(\cdot, t) \in H^{1,2}(I)$ and $w(\cdot, t) \in H_0^{1,2}(I)$ such that $u_t(\cdot, t) \in H^{1,2}(I)$, $u(0, t) = \alpha$, $u(1, t) = \beta$, $u(\cdot, 0) = u_0$, and

$$\int_I \frac{u_t}{\sqrt{1 + u_x^2}}\varphi\, dx = -\int_I g'(u_x)\varphi_x\, dx - \varepsilon^2 \int_I w^2 \frac{u_x\varphi_x}{(1 + u_x^2)^{3/2}} - 2\frac{w_x\varphi_x}{(1 + u_x^2)^{3/2}}\, dx \quad \forall \varphi \in H_0^{1,2}(I), \tag{10}$$

$$\int_I \frac{w}{\sqrt{1 + u_x^2}}\psi\, dx = -\int_I \frac{u_x}{\sqrt{1 + u_x^2}}\psi_x\, dx \qquad \forall \psi \in H_0^{1,2}(I) \tag{11}$$

for almost every time $t \in [0, T_\varepsilon]$.

Note that the classical version of the flow is the one given by (4) subject to the boundary conditions $u(0,t) = \alpha$, $u(1,t) = \beta$, $u_{xx}(0,t) = u_{xx}(1,t) = 0$ (natural boundary conditions) and to the initial data $u(\cdot, 0) = u_0$.

The above mixed formulation is derived by computing the first variation of the energy functional in such a way that no integration by parts is needed. As a consequence it is easy to show that in the semi-discrete setting the energy decreases along the flow (see [8] and references given in there for more details).

The non-convexity of the anisotropy function leads to very interesting phenomena. Indeed, for small ε, it is natural to expect a "heat-equation-like" evolution in those part of the domain where the map g is convex. In those regions where this is not the case one has to be more watchful. Thus we define (cf. also [5]) the *globally* and *locally* unstable set

$$\mathrm{GUS} := \{y \in \mathbb{R} : g(y) > g^{**}(y)\} \qquad \supset \qquad \mathrm{LUS} := \{y \in \mathbb{R} : g''(y) < 0\}.$$

The (closed) set where g and its convex envelope g^{**} coincide is the *globally stable* set

$$\mathrm{GS} := \mathbb{R} \setminus \mathrm{GUS} = \{y \in \mathbb{R} : g^{**}(y) = g(y)\}.$$

3 LONGTIME EVOLUTION AND TIME RESCALING

In [3], where a related problem is thoroughly discussed, the authors suggested that one can divide the evolution into three phases: a first (very) short period of time characterized by wrinkles formation and a drastic drop in the energy, a second one in which the non wrinkled regions evolve in a "heat-equation" manner (at this stage the wrinkled region contributes to so little energy that motion herein is *extremely* slow), and a third one which is characterized by the motion of the free boundary separating the wrinkled from the unwrinkled region. The experiments done for our model indicate that we can adopt a similar point of view.

As mentioned in the Introduction we intend to focus here on the evolution *after* the formation of wrinkles (experimentally analyzed in [8]). One way to "quickly go past" the first phase is obtained by performing a time rescaling. The rescaling $\tau = \frac{t}{\varepsilon}$ (with small ε) obviously transforms (4) into

$$\frac{u_\tau}{\sqrt{1+u_x^2}} = \frac{1}{\varepsilon} g''(u_x) u_{xx} - \frac{\varepsilon}{(1+u_x^2)^{1/2}} \left(2\frac{u_{xxxx}}{(1+u_x^2)^2} - 20\frac{u_x u_{xx} u_{xxx}}{(1+u_x^2)^3} + \frac{u_{xx}^3}{(1+u_x^2)^4}(30u_x^2 - 5) \right),$$

whereas the rescaling $\tau = \frac{t}{\varepsilon^2}$ gives

$$\frac{u_\tau}{\sqrt{1+u_x^2}} = \frac{1}{\varepsilon^2} g''(u_x) u_{xx} - \frac{1}{(1+u_x^2)^{1/2}} \left(2\frac{u_{xxxx}}{(1+u_x^2)^2} - 20\frac{u_x u_{xx} u_{xxx}}{(1+u_x^2)^3} + \frac{u_{xx}^3}{(1+u_x^2)^4}(30u_x^2 - 5) \right).$$

Thus for simplicity we will describe the flow as

$$\begin{aligned} \frac{u_t}{\sqrt{1+u_x^2}} &= \Psi(\text{ weighted length term }) - \Upsilon(\text{ Willmore term }) \qquad (12) \\ &= \Psi g''(u_x) u_{xx} - \frac{\Upsilon}{(1+u_x^2)^{1/2}} \left(2\frac{u_{xxxx}}{(1+u_x^2)^2} - 20\frac{u_x u_{xx} u_{xxx}}{(1+u_x^2)^3} + \frac{u_{xx}^3}{(1+u_x^2)^4}(30u_x^2 - 5) \right) \end{aligned}$$

where Ψ and Υ correspond to a chosen ε-rescaling and will be specified for each numerical experiment.

4 WRINKLES PHENOMENA

Similarly to [3] (cf. also [5]) we have observed that the flow develops wrinkles very early in the stage of the evolution and that these wrinkles do not leave the region

$$\Sigma_L(u_0) := \{x \in [0,1] \,:\, u_{0x}(x) \in \mathrm{LUS}\},$$

where u_0 is the given initial curve. A plausible explanation for the wrinkles phenomena is given in [3] (see also [8, § 7]). In the following we briefly sketch the main arguments for the sake of the reader.

We know that lines $\bar{u}(x) = px + q$, $x \in [0,1]$, $p, q \in \mathbb{R}$, are stationary solutions for the flow for any choice of ε (their stability or instability depending on the value p and the choice of anisotropy). We might therefore assume that, for perturbed initial data, say $\bar{u} + \delta\bar{v}(\cdot, \varepsilon)$, a solution to the flow is of type

$$u(x,t,\varepsilon;\delta) = \bar{u}(x) + \delta v(x,t,\varepsilon) + \mathcal{O}(\delta^2)$$

for small δ. Plugging the above expression into (12), dividing by δ, and choosing $\delta = 0$, we observe that v has to satisfy the linear PDE

$$v_t = \Psi g''(p) v_{xx}\sqrt{1+p^2} - 2\Upsilon \frac{v_{xxxx}}{(1+p^2)^2}.$$

Looking for solutions of type $v(x,t,\varepsilon) = \exp(\lambda t)\sin(mx)$, we see that $\lambda = \lambda(\varepsilon)$ and $m = m(\varepsilon)$ must satisfy the relation

$$\lambda = -m^2\left(\frac{2\Upsilon}{(1+p^2)^2}m^2 + \Psi g''(p)\sqrt{1+p^2}\right).$$

Thus we notice that if g is convex then λ is negative and oscillations can be basically neglected. On the contrary, if $g''(p) < 0$ then we see that λ is positive provided that $m^2 < -\frac{\Psi}{\Upsilon}\frac{g''(p)}{2}(1+p^2)^{5/2}$. More precisely λ assumes it maximum value

$$\lambda_{\max} = \Psi\frac{\Psi}{\Upsilon}\frac{(g''(p))^2}{8}(1+p^2)^3 \tag{13}$$

at

$$m^2_{\max} = -\frac{\Psi}{\Upsilon}\frac{g''(p)}{4}(1+p^2)^{5/2}. \tag{14}$$

Note that for the considered flows the ratio

$$\frac{\Psi}{\Upsilon} = \frac{1}{\varepsilon^2} \tag{15}$$

is independent of the chosen time rescaling (and therefore this is true also for the wavelength of v). On the other hand $\lambda_{\max}$ is of order $\frac{1}{\varepsilon^2}$, $\frac{1}{\varepsilon^3}$, $\frac{1}{\varepsilon^4}$ depending whether we are considering the original problem or the rescaled one with $\tau = \frac{t}{\varepsilon}$ and $\tau = \frac{t}{\varepsilon^2}$ respectively. In any case we can expect to observe the oscillatory term v very rapidly, and even more so by every time rescaling.

Next, thinking of a flow with initial curve u_0, we can assume that locally around $x_0 \in [0,1]$ the initial map can be approximated by its linear part $u_{0x}(x_0)(x - x_0) + u_0(x_0)$. Assuming that the above analysis applies, we expect the wrinkles phenomenon to appear only in the region $\Sigma_L(u_0) = \{x \in [0,1] \,:\, u_{0x}(x) \in \mathrm{LUS}\}$ as stated above. Furthermore the expression for $m_{\max}$ suggests that the wave length of the appearing wrinkles should be $\mathcal{O}(\varepsilon)$.

5 THE DISCRETE SCHEME

Based on (10) – (11), we proposed in [8] the following semi-implicit scheme, which we use also for the experiments shown in this paper.

Let $\bar{I} = \bigcup_{j=1}^{N+1} I_j$ be a decomposition of the interval $\bar{I} = [0,1]$ into intervals $I_j = [x_{j-1}, x_j]$ for $j = 1, \dots, N+1$. We set $x_0 = 0$ and $x_{N+1} = 1$. Let $h_j = |I_j|$ and $h = \max_{j=1,\dots,N+1} h_j$ be the maximal diameter of a grid element. We assume that for some constant $\tilde{c} > 0$ we have that $h_j \geq \tilde{c}h$. In practice we will use equidistant grid points so that $h = h_j$ for all $j = 1, \dots, N+1$. We introduce the finite dimensional space

$$X_h := \{v \in C^0(\bar{I}, \mathbb{R}) \,:\, v|_{I_j} \in P_1(\bar{I}_j),\, j = 1, \cdots, N+1\}$$

of continuous piecewise affine functions on the grid. The $N+2$ scalar nodal basis functions $\varphi_j \in X_h$ are defined by $\varphi_j(x_i) = \delta_{ij}$. Let $X_h^0 := \text{span}\{\varphi_1, \dots, \varphi_N\}$ and I_h be the usual linear interpolation operator. Let τ be the time step. For a generic function f we denote its evaluation at the m-th time level $t^m = m\tau$ by $f^m = f(\cdot, t^m)$.

The discrete problem can be formulated as follows: compute $u_h^{m+1} \in X_h$ and $w_h^{m+1} \in X_h^0$ so that $u_h^{m+1}(0) = \alpha$, $u_h^{m+1}(1) = \beta$ and

$$\int_I \frac{u_h^{m+1} - u_h^m}{\tau} \frac{\varphi_h}{Q_h^m} + \Psi \int_I g'(u_{hx}^m)\varphi_{hx} + \Upsilon \left(\int_I \frac{(w_h^m)^2}{(Q_h^m)^3} u_{hx}^{m+1} \varphi_{hx} - 2 \int_I \frac{w_{hx}^{m+1}}{(Q_h^m)^3} \varphi_{hx} \right) = 0 \tag{16}$$

for all $\varphi_h \in X_h^0$, and

$$\int_I \frac{w_h^{m+1}}{Q_h^m} \psi_h + \int_I \frac{u_{hx}^{m+1}}{Q_h^m} \psi_{hx} = 0 \qquad \forall \psi_h \in X_h^0\,, \tag{17}$$

where $Q_h^m = \sqrt{1 + (u_{hx}^m)^2}$. As initial data we use $u_h^0 = I_h u_0$ and w_h^0, which is computed from

$$\int_I \frac{w_h^0}{Q_h^0} \psi_h + \int_I \frac{u_{hx}^0}{Q_h^0} \psi_{hx} = 0 \qquad \forall \psi_h \in X_h^0\,.$$

Thus we have to solve a linear system in each time iteration (more details in [8]).

6 NUMERICAL EXPERIMENTS

For all experiments shown here we choose

$$h = 10^{-3} \qquad \text{and} \qquad \tau = 100h^4 = 10^{-10}.$$

We consider the anisotropy function from [8, § 9.2]

$$g(y) = \begin{cases} \frac{1}{8}(y-1)^2(y+1)^2 + 1, & |y| \leq 1, \\ \sqrt{1 + (|y|-1)^2}, & |y| > 1, \end{cases}$$

taking its minima at ± 1, see Figure 1.

A straightforward computation gives

$$g'(y) = \begin{cases} \frac{1}{2}y(y^2-1), & |y| < 1, \\ \frac{(|y|-1)}{\sqrt{1+(|y|-1)^2}} \operatorname{sign}(y), & |y| > 1, \end{cases} \qquad g''(y) = \begin{cases} \frac{1}{2}(3y^2-1), & |y| < 1, \\ \frac{1}{(1+(|y|-1)^2)^{3/2}}, & |y| > 1. \end{cases}$$

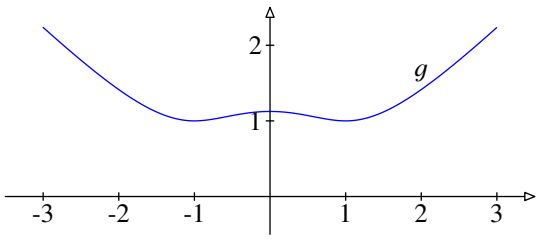

Figure 1: The anisotropy function used for the experiments.

Note that $g \in C^2(\mathbb{R})$, and $g''(y) = 0$ if and only if $y = \pm\frac{1}{\sqrt{3}}$. Thus we have that

$$\mathrm{LUS} = \left(-\frac{1}{\sqrt{3}}, \frac{1}{\sqrt{3}}\right), \qquad \mathrm{GUS} = (-1, 1). \tag{18}$$

We stop our computations whenever the energy starts to oscillate, even so slightly (when this happens, it is usually after some coarsening of the microstructures and in the proximity of a wrinkled curve with a shape similar to that of a possible equilibrium). We conjecture such behavior to be a consequence of stability issues and round-off errors. A smaller time step is theoretically more appropriate but it would be at expenses of the computational time.

6.1 Wavelength

As initial data for the tests discussed in Sections 6.1.1, 6.1.2, and 6.1.4 we choose

$$u_0(x) = \frac{\sin(2\pi x)}{20\pi} \tag{19}$$

which has also been considered in [8, Test 3]. Its slope amounts to $u_0'(x) = \frac{1}{10}\cos(2\pi x)$ which gives $\Sigma_L(u_0) = [0, 1]$. Thus we expect microstructures to appear in the whole interval.

To give an estimate for the number of wrinkles nw, we proceed as in [3] (see also [8]): since $|u_0'| \le \frac{1}{10} \ll 1$ for all $x \in [0, 1]$, we may take $p = 0$ into (14) and using the fact that $g''(0) = -\frac{1}{2}$ we obtain the approximation

$$\mathrm{nw} \approx \frac{m_{\max}}{2\pi} = \frac{1}{4\sqrt{2}\pi}\sqrt{\frac{\Psi}{\Upsilon}}. \tag{20}$$

In view of (15) this quantity does not depend on time rescaling as remarked in Section 4.

6.1.1 Merging of wrinkles

In our previous paper [8, Test 3] we investigated for the initial data (19) evolution of type $(\Psi, \Upsilon) = (1, \varepsilon^2)$. Here we consider the time rescaled version $(\Psi, \Upsilon) = (\frac{1}{\varepsilon}, \varepsilon)$ with $\varepsilon = \frac{1}{500}$, thus $(\Psi, \Upsilon) = (500, \frac{1}{500})$. We obtain $\mathrm{nw} \approx 28.1$.

Time shots of the evolution and the energy plot are shown in Figure 2. The first five shots qualitatively correspond to the plots in [8, Figure 10]. The wrinkles invade the interval from the boundary points. At time $t = 5 \cdot 10^{-5}$ the formation of wrinkles appears to be completed and one can observe how accurate is the prediction $\mathrm{nw} \approx 28.1$.

The time rescaling allows us to compute (a good part of) the evolution *after* the formation of wrinkles in a reasonable time. Here we face a merging phenomenon which occurs in several discrete steps and leads to a doubling of wavelength.

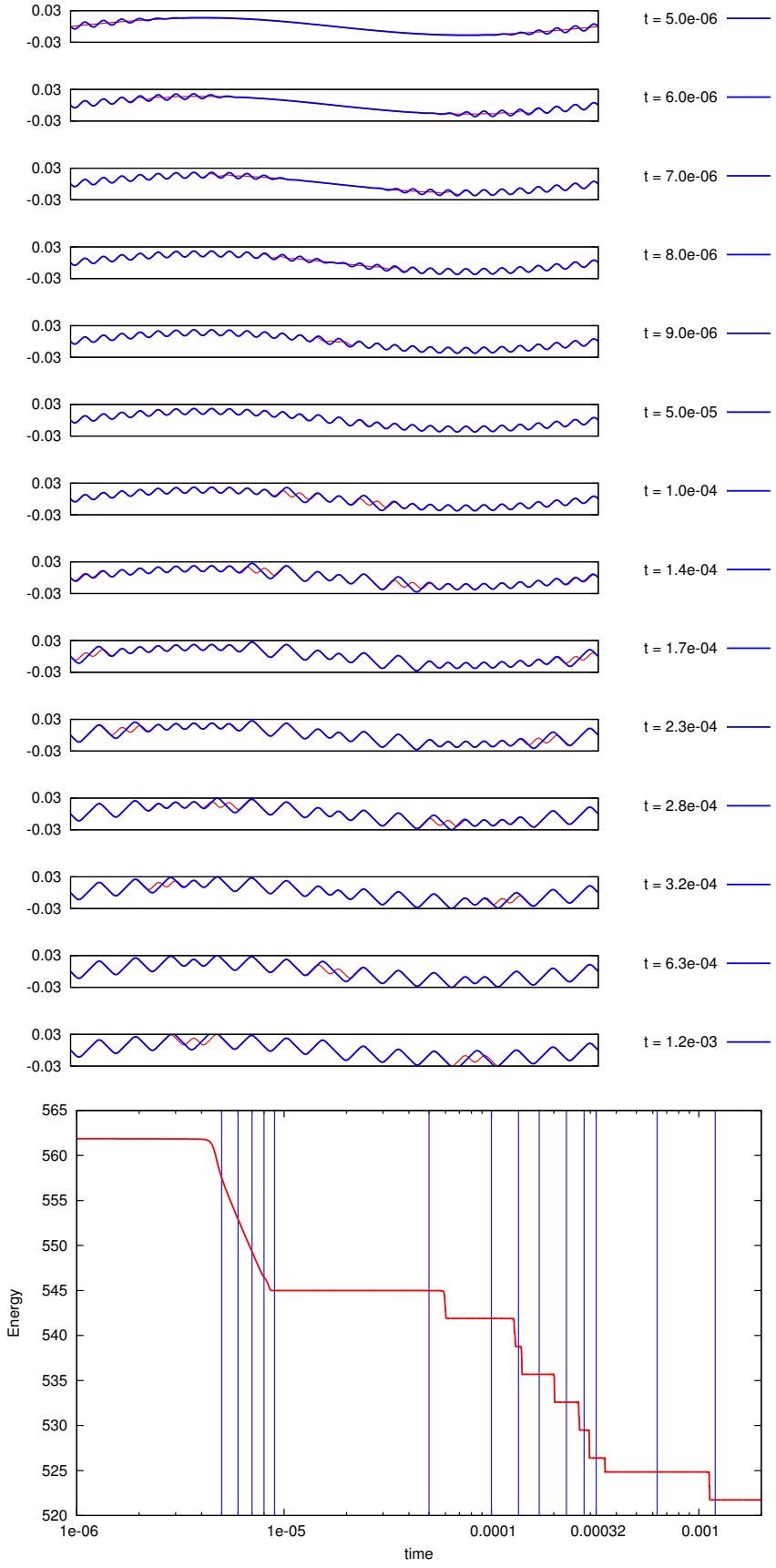

Figure 2: Merging of wrinkles. The red curve in the time step portraits above refers to the plot immediately above. The plots are true to scale. The vertical blue lines in the energy plot below correspond to the time step portraits. Be aware of the log-scale for the time coordinate.

6.1.2 Superimposition of waves

We perform two tests, namely $(\Psi, \Upsilon) = (2500, 1)$ and $(\Psi, \Upsilon) = (4000, 1)$ which leads to $\mathrm{nw} \approx 2.8$ and $\mathrm{nw} \approx 3.6$ respectively. Plots are shown in Figures 3 and 4.

We mainly observe the following two facts.

a) When nw is small and the initial curve is a "wave" itself, it might be harder to confirm the predicted number of wrinkles. However, at a certain stage of the evolution, the curve is in fact a superimposition of sines, one having the same wavelength as the original curve and another with wavelength according to $m_{\max}$, see Section 4.

b) A relatively small change in the predicted number of wrinkles (2.8 vs. 3.6) may lead to big differences in the evolution. Compare Figure 3 vs. 4.

6.1.3 Perturbed initial data

In order to break symmetry we add a small "bump" to (19), so we consider the perturbed initial data

$$\tilde{u}_0(x) = u_0(x) + b(x)$$

drawn in Figure 5 (top), where

$$b(x) = 40 \exp\left(-\frac{1}{x^2}\right) \exp\left(-\frac{1}{(1-x)^2}\right).$$

In order to show $\Sigma_L(\tilde{u}_0) = [0, 1]$ we first compute the derivatives

$$b'(x) = 80 \exp\left(-\frac{1}{x^2}\right) \exp\left(-\frac{1}{(1-x)^2}\right) \cdot \left(\frac{1}{x^3} - \frac{1}{(1-x)^3}\right),$$

$$b''(x) = 80 \exp\left(-\frac{1}{x^2}\right) \exp\left(-\frac{1}{(1-x)^2}\right) \cdot \left[2\left(\frac{1}{x^3} - \frac{1}{(1-x)^3}\right)^2 - \frac{3}{x^4} - \frac{3}{(1-x)^4}\right].$$

The second derivative vanishes if and only if the bracket $[\cdots]$ is zero which is equivalent to

$$6\,x^8 - 24\,x^7 + 40\,x^6 - 36\,x^5 + 3\,x^4 + 26\,x^3 - 27\,x^2 + 12\,x - 2 = 0.$$

This equation possesses in $[0, 1]$ precisely the two roots $x_0 \approx 0.42541$ and $1 - x_0 \approx 0.57459$. From $b'(0) = b'(1) = 0$ and $b'(1 - x_0) = -b'(x_0)$ we deduce $|u_0'| \leq \frac{1}{10} + b'(x_0) \approx 0.21895$ which clearly is smaller than $\frac{1}{\sqrt{3}} \approx 0.57735$.

Letting $(\Psi, \Upsilon) = (2500, 1)$, the situation is similar to the first case from Section 6.1.2.

Interestingly, the time shots of the flow for $t > 0$ look quite symmetric, so the non-symmetry of the initial curve is not reflected by the evolution.

6.1.4 The length of the first time scale

Let $T = T(\varepsilon)$ denote the time where wrinkles have emerged but not yet merged, e. g. $t = 10^{-5}$ in Figure 2. (In previous experiments [8, Test 3] we considered the time at which the energy *starts* to drop.)

As already observed [3, § 6.4] (see also (13)) we expect $T(\varepsilon) = \mathcal{O}(\varepsilon^2)$ for $(\Psi, \Upsilon) = (1, \varepsilon^2)$. Rescaling the time leads to $T(\varepsilon) = \mathcal{O}(\varepsilon^3)$ for $(\Psi, \Upsilon) = (\frac{1}{\varepsilon}, \varepsilon)$ and $T(\varepsilon) = \mathcal{O}(\varepsilon^4)$ for $(\Psi, \Upsilon) = (\frac{1}{\varepsilon^2}, 1)$.

In Table 1 we compare the respective values for $T(\varepsilon)$ from our previous simulations [8] with the corresponding tests in the $(\frac{1}{\varepsilon}, \varepsilon)$ setting. For the $(\frac{1}{\varepsilon^2}, 1)$ rescaling this is not possible as the expected values are too close to the time step size to read off sufficiently exact data.

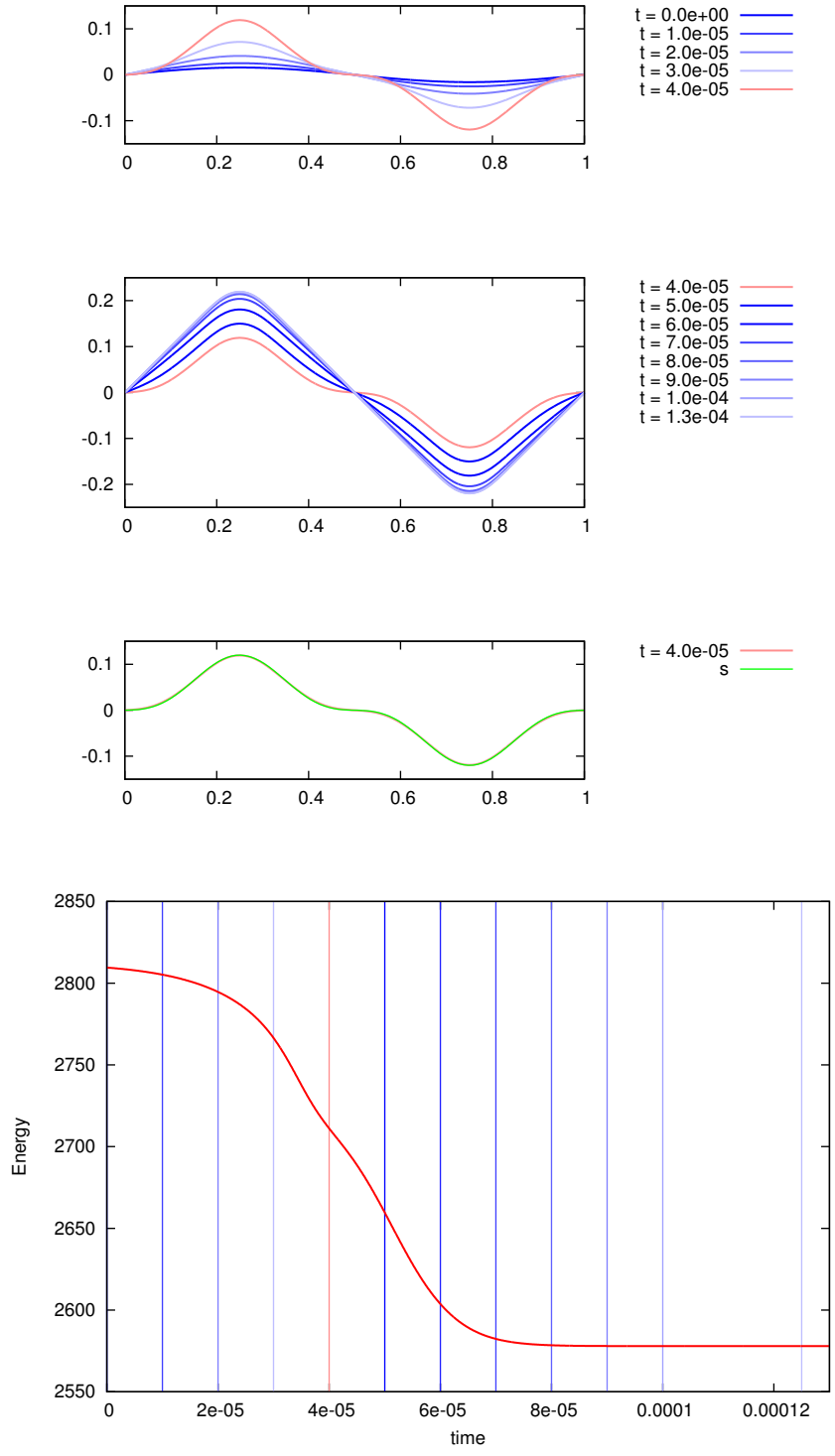

Figure 3: Superimposition of a wave by ≈ 2.8 wrinkles (first case $\Psi = 2500$). The first two diagrams show the evolution of the curve before and after $t_0 = 4 \cdot 10^{-5}$. The third diagram compares the curve at time t_0 with $s(x) = \frac{1}{11} \sin 2\pi x - \frac{1}{11\pi} \sin 6\pi x$. The vertical lines in the energy plot below correspond to the time step portraits drawn in the diagrams above.

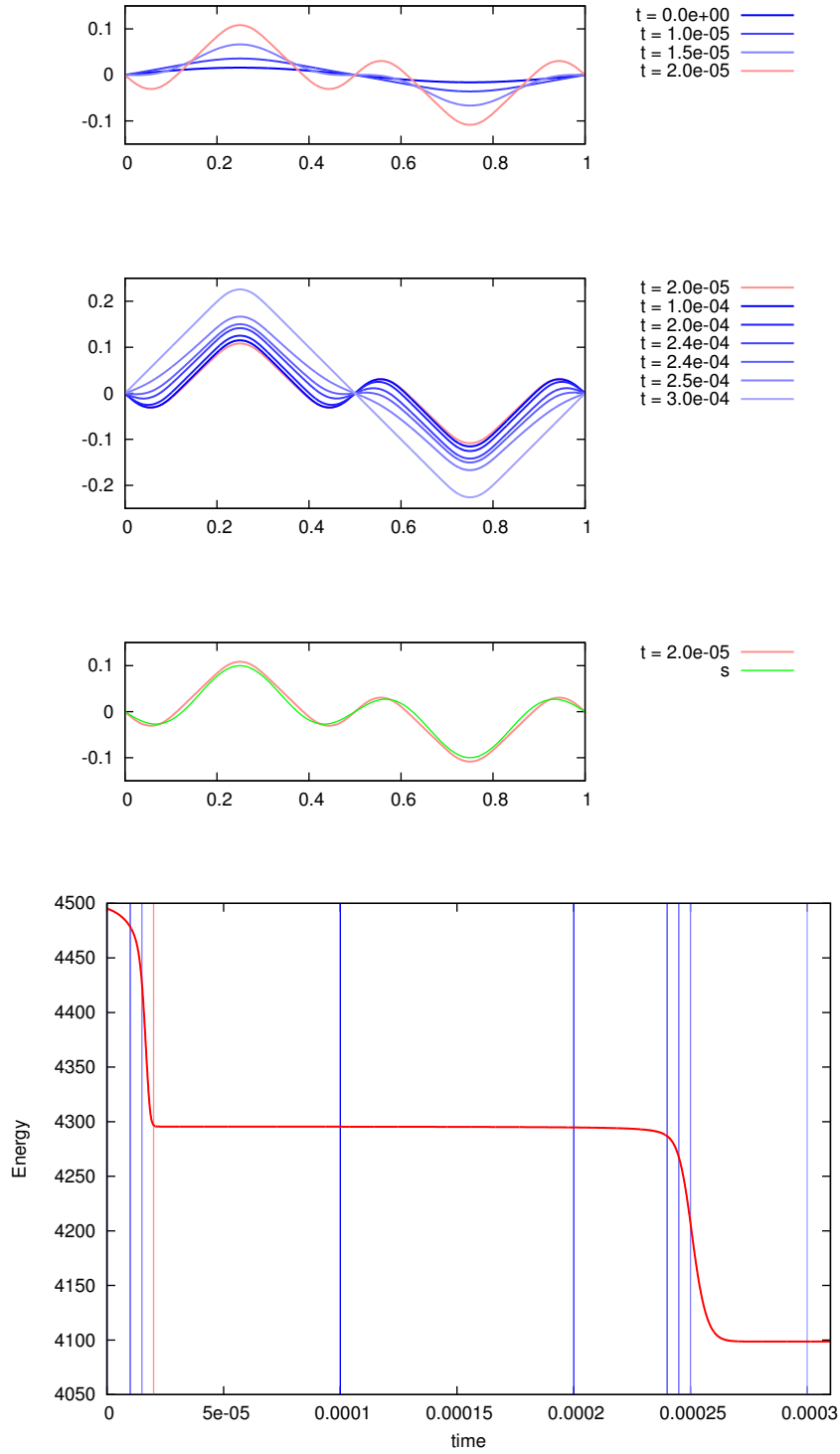

Figure 4: Superimposition of a wave by ≈ 3.6 wrinkles (second case $\Psi = 4000$). The first two diagrams show the evolution of the curve before and after $t_0 = 2 \cdot 10^{-5}$. The third diagram compares the curve at time t_0 with $s(x) = \frac{1}{20} \sin 2\pi x - \frac{1}{20} \sin 6\pi x$. The vertical lines in the energy plot below correspond to the time step portraits drawn in the diagrams above.

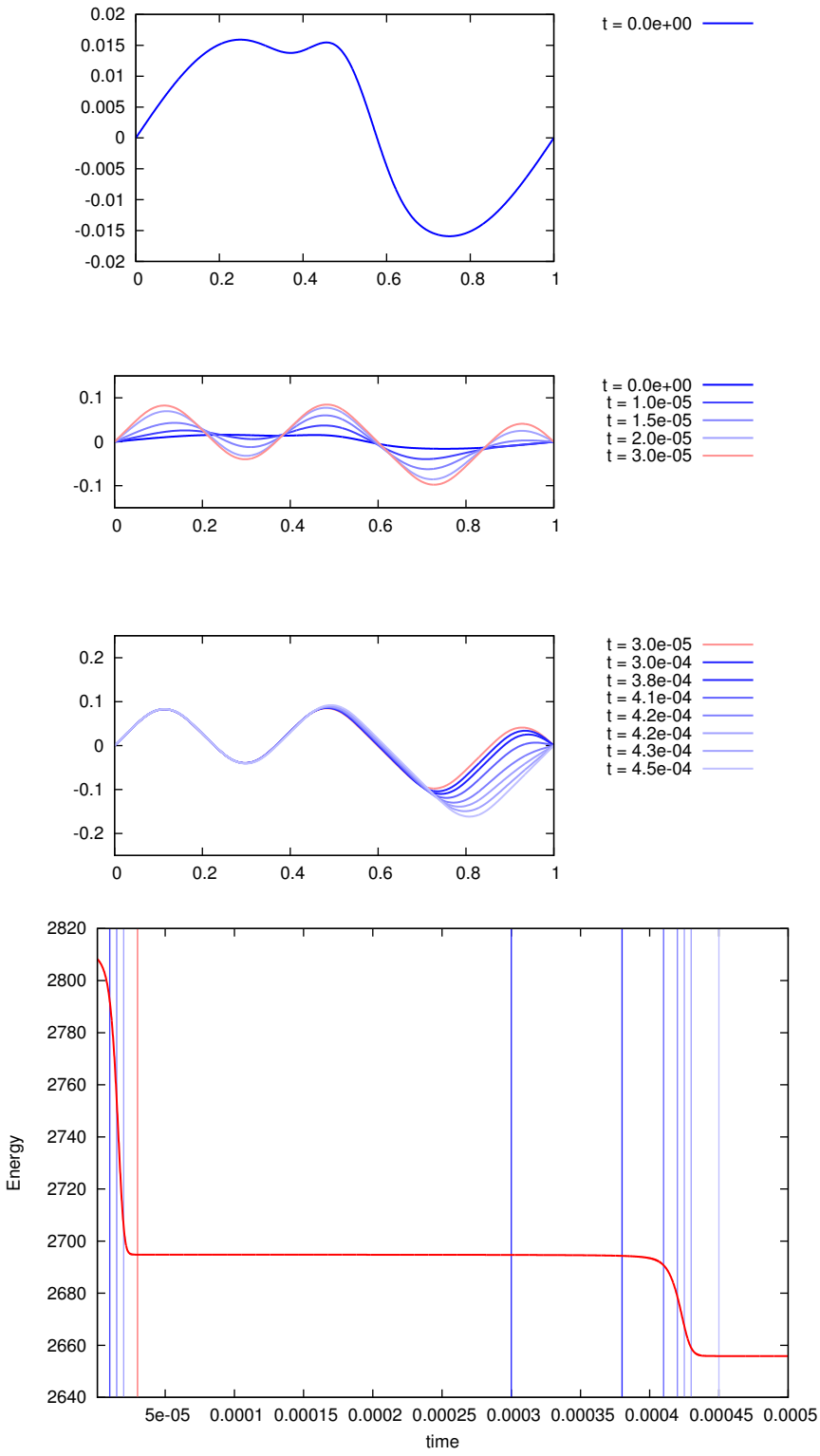

Figure 5: Perturbed initial data. The first diagram shows the initial curve. Note the different scaling of x- and y-axis. The following diagrams show the evolution before and after $t_0 = 3 \cdot 10^{-5}$ and the energy plot below. As in Figure 3 we expect about 3 wrinkles to appear.

(Ψ, Υ)	$(1, \varepsilon^2)$	$(\varepsilon^{-1}, \varepsilon)$	$(\varepsilon^{-2}, 1)$
$\varepsilon = 5 \cdot 10^{-4}$	$2.8 \cdot 10^{-4}$	$1.4 \cdot 10^{-7}$	—
$\varepsilon = 1 \cdot 10^{-3}$	$1.1 \cdot 10^{-3}$	$1.2 \cdot 10^{-6}$	—
$\varepsilon = 2 \cdot 10^{-3}$	$4.2 \cdot 10^{-3}$	$8.7 \cdot 10^{-6}$	$2.2 \cdot 10^{-8}$
experimental power	1.95	2.98	—

Table 1: Time values $T(\varepsilon)$ at which wrinkles have emerged but not yet merged and thus the first time scale has ended. The experimental power is computed by linear interpolation in a log-log scale, see Figure 6.

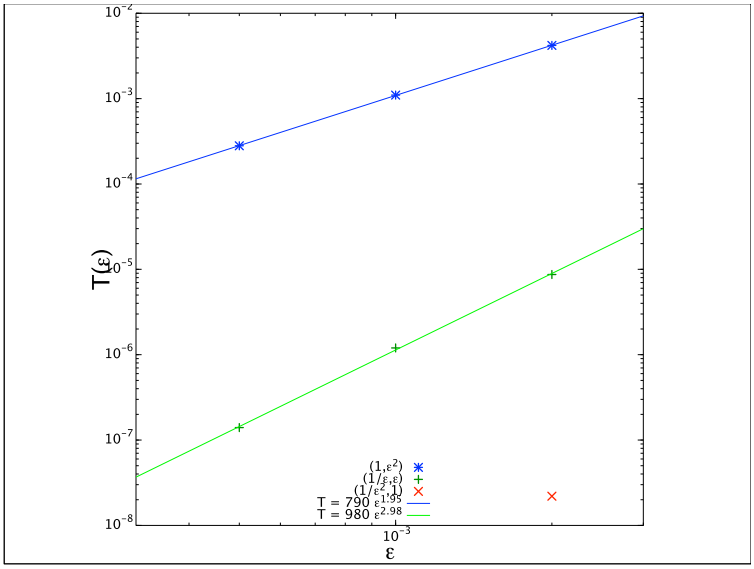

Figure 6: Visualization of the values in Table 1.

6.2 WV-curves

Here we choose the initial curve to be a perturbation of a stationary solution. Precisely we take

$$u_0(x) = \begin{cases} -x, & x \in [0, \frac{1}{4} - \frac{r}{\sqrt{2}}], \\ -\frac{1}{4} + \sqrt{2}r - \sqrt{r^2 - (x - \frac{1}{4})^2}, & x \in (\frac{1}{4} - \frac{r}{\sqrt{2}}, \frac{1}{4} + \frac{r}{\sqrt{2}}), \\ x - \frac{1}{2}, & x \in [\frac{1}{4} + \frac{r}{\sqrt{2}}, 1], \end{cases}$$

where $r = \frac{3}{8(\sqrt{2}+\sqrt{5}/2)}$. The initial curve is depicted in Figure 7 (top).

In this case $\Sigma_L(u_0) = (-\frac{1}{2}r + \frac{1}{4}, \frac{1}{2}r + \frac{1}{4}) \approx (0.176, 0.324)$.

The evolutions for $(\Psi, \Upsilon) = (500, \frac{1}{500})$ and $(\Psi, \Upsilon) = (200, \frac{1}{200})$ are depicted in Figures 7 and 8.

In the first case we observe a merging process similar to Section 6.1.1. The relatively large value $\varepsilon = \frac{1}{200}$ does not permit the evolution of clearly visible wrinkles in the second case, however the curve at $t = 10^{-5}$ is almost concave about $x = \frac{1}{4}$ which could reflect a superimposition by two wrinkles.

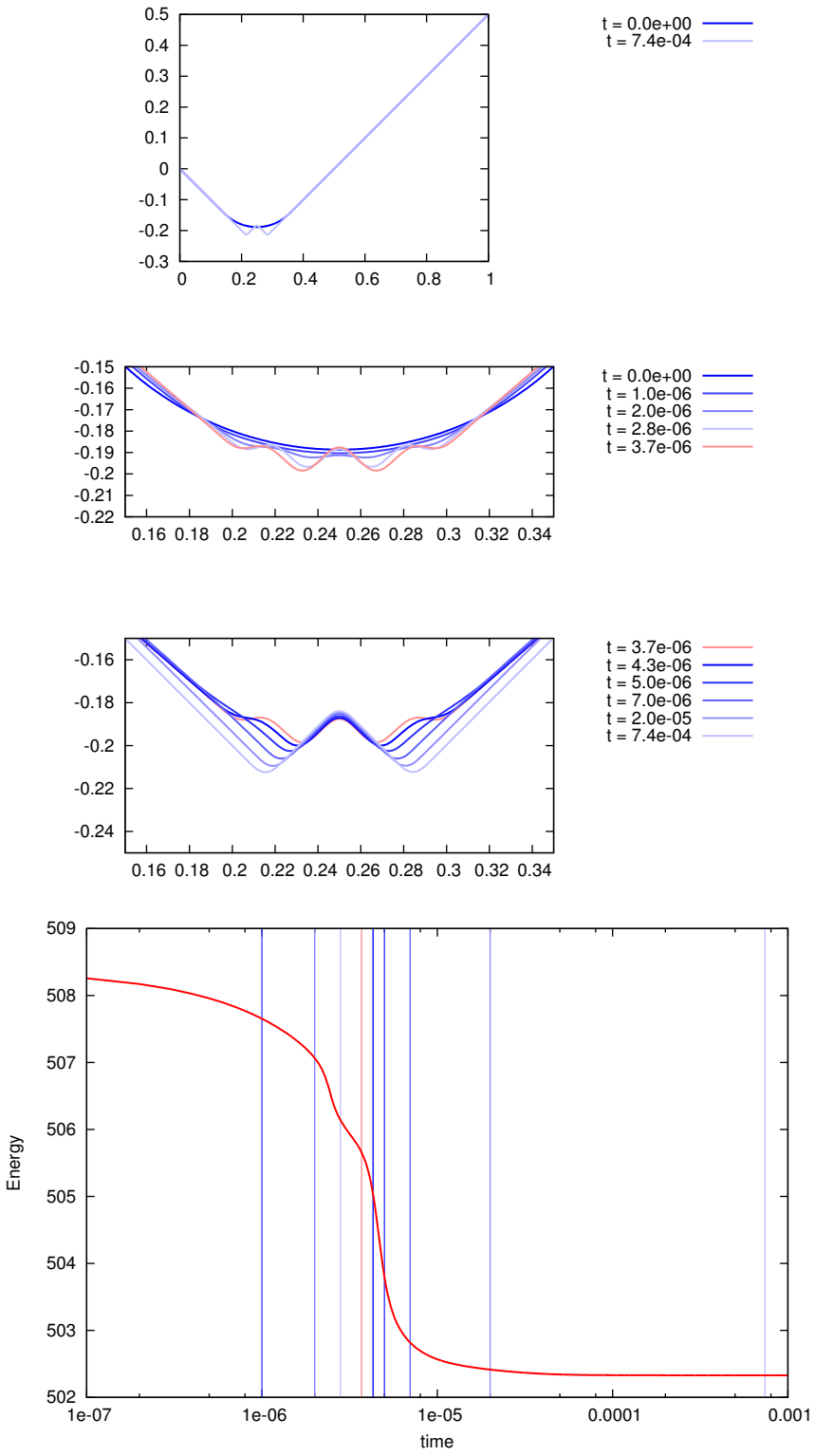

Figure 7: The W-curve (first case $\Psi = 500$). The first diagram shows the initial curve versus the state after evolution of wrinkles. Time shots of the evolution in the interval $[0.15, 0.35]$ before and after $t_0 = 3.7 \cdot 10^{-6}$ are followed by the energy plot (log-scale for the time coordinate).

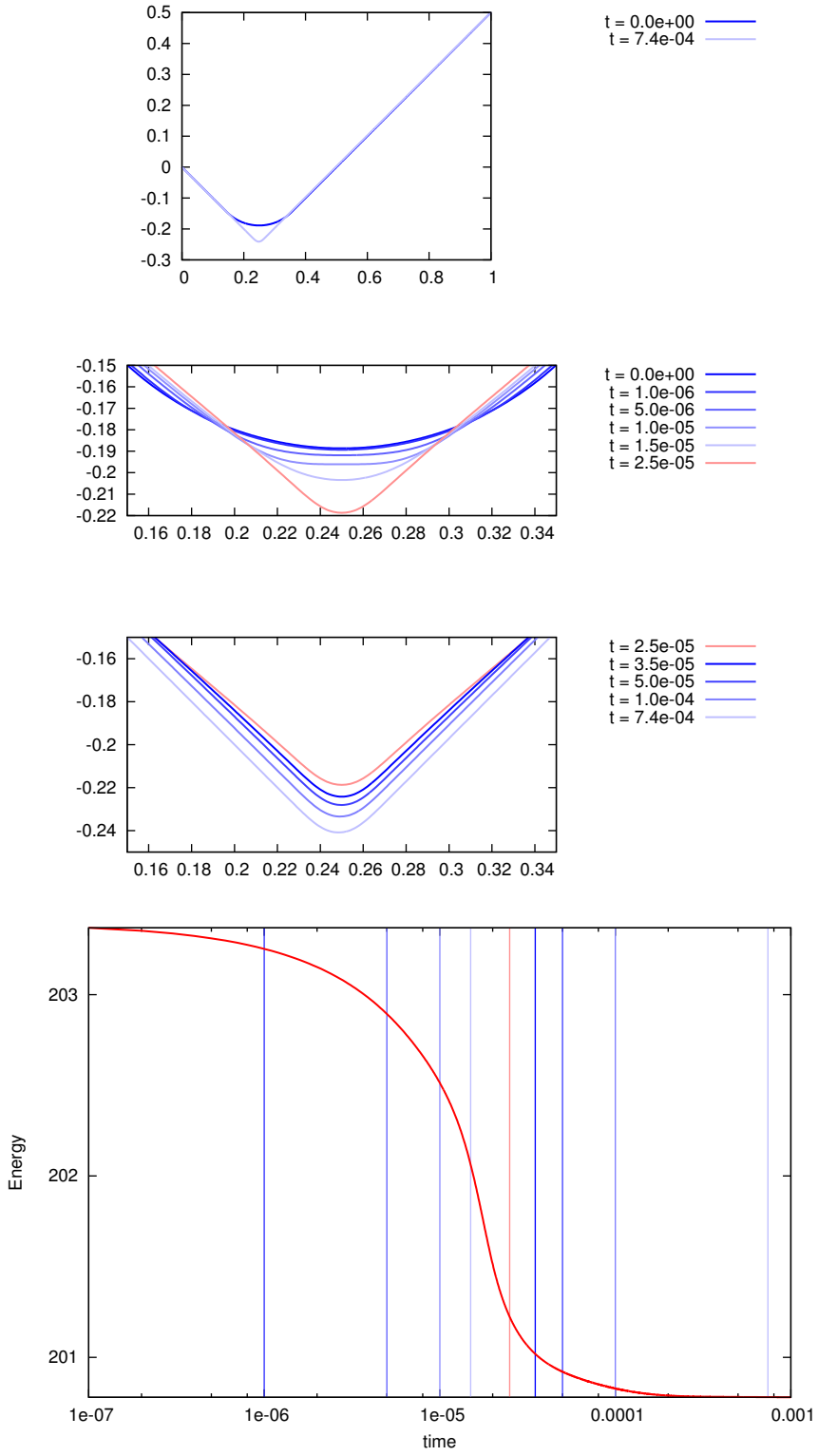

Figure 8: The V-curve (second case $\Psi = 200$). The first diagram shows the initial curve versus the state after evolution of wrinkles. Time shots of the evolution in the interval $[0.15, 0.35]$ before and after $t_0 = 2.5 \cdot 10^{-5}$ are followed by the energy plot (log-scale for the time coordinate).

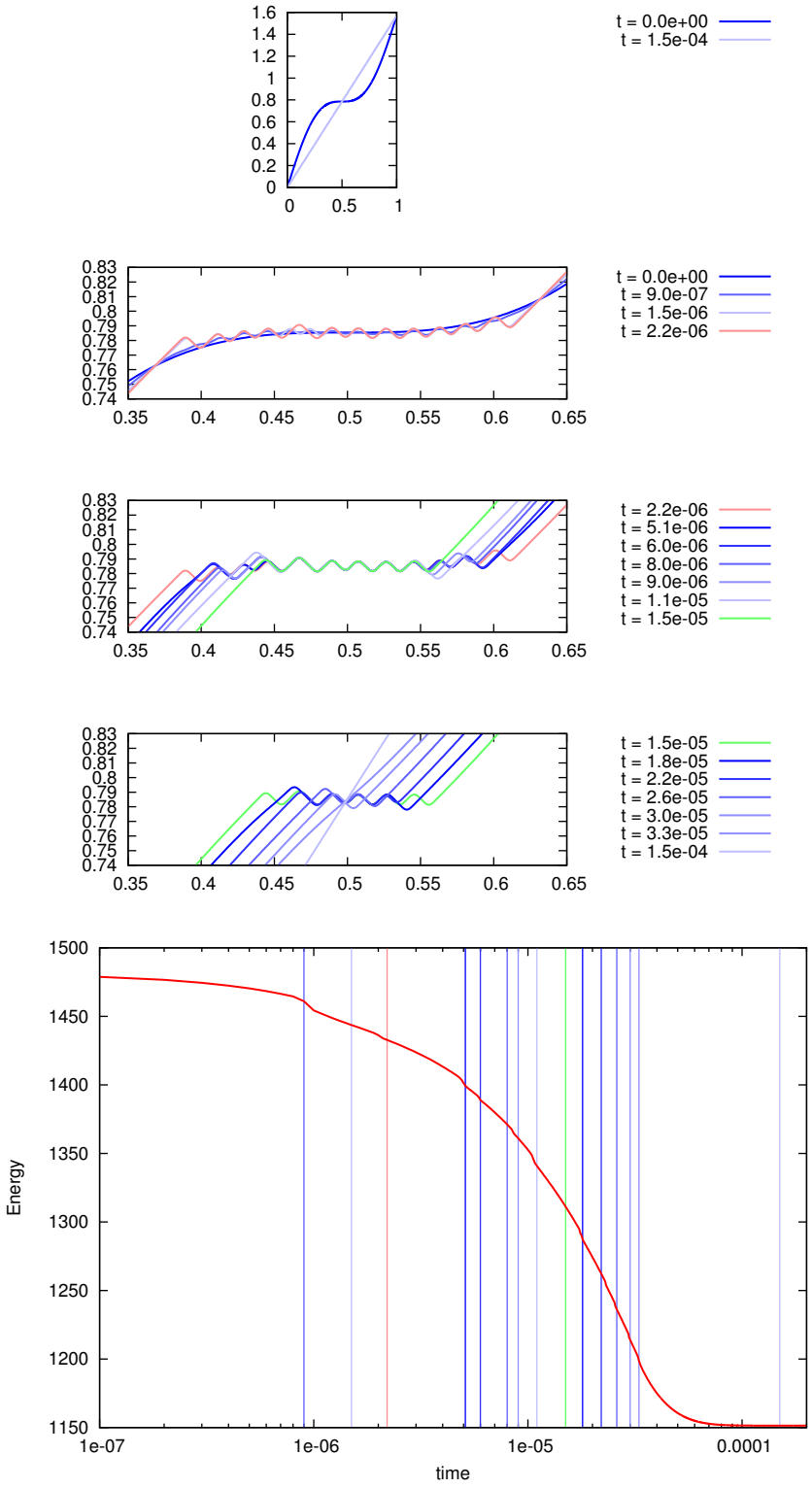

Figure 9: Long-time evolution. Be aware of the log-scale for the time coordinate in the energy plot.

6.3 Long-time evolution

As initial data we choose

$$u_0(x) = \tfrac{1}{4}\sin 2\pi x + \tfrac{1}{2}\pi x$$

which has also been considered in [3, § 6.2] and [8, Test 6]. A straightforward calculation gives $\Sigma_L(u_0) = (x_L, 1-x_L)$, where $x_L = \frac{1}{2\pi}\arccos(\frac{2}{\pi\sqrt{3}} - 1) \approx 0.359$. We consider the evolution for $(\Psi, \Upsilon) = (1000, \frac{1}{1000})$, obtaining better resolved wrinkles than in our previous experiment [8, Test 6] where $(\Psi, \Upsilon) = (1, 10^{-8})$ and $\tau = 10^{-8}$. The initial curve evolves to an equilibrium.

REFERENCES

[1] Sigurd Angenent and Morton E. Gurtin. Multiphase thermomechanics with interfacial structure. II. Evolution of an isothermal interface. *Arch. Rational Mech. Anal.*, 108(4):323–391, 1989.

[2] Giovanni Bellettini and Giorgio Fusco. The Γ-limit and the related gradient flow for singular perturbation functionals of Perona-Malik type. *Trans. Amer. Math. Soc.*, 360(9):4929–4987, 2008.

[3] Giovanni Bellettini, Giorgio Fusco, and Nicola Guglielmi. A concept of solution and numerical experiments for forward-backward diffusion equations. *Discrete Contin. Dyn. Syst.*, 16(4):783–842, 2006.

[4] Antonio Di Carlo, Morton E. Gurtin, and Paolo Podio-Guidugli. A regularized equation for anisotropic motion-by-curvature. *SIAM J. Appl. Math.*, 52(4):1111–1119, 1992.

[5] Francesca Fierro, Roberta Goglione, and Maurizio Paolini. Numerical simulations of mean curvature flow in the presence of a nonconvex anisotropy. *Math. Models Methods Appl. Sci.*, 8(4):573–601, 1998.

[6] Morton E. Gurtin. *Thermomechanics of evolving phase boundaries in the plane*. Oxford Mathematical Monographs. The Clarendon Press Oxford University Press, New York, 1993.

[7] Morton E. Gurtin and Michel E. Jabbour. Interface evolution in three dimensions with curvature-dependent energy and surface diffusion: interface-controlled evolution, phase transitions, epitaxial growth of elastic films. *Arch. Ration. Mech. Anal.*, 163(3):171–208, 2002.

[8] Paola Pozzi and Philipp Reiter. Mean curvature flow in the presence of a non-convex anisotropy: Willmore type regularization in the graph setting. Preprint 1-11, Fakultät für Mathematik und Physik, Universität Freiburg, 2011.